Design and Development of Low-Loss Transformer for Powering Small Implantable Medical Devices

Kenji Shiba, *Member, IEEE*, Akira Morimasa, and Harutoyo Hirano

***Abstract*—Small implantable medical devices, such as wireless capsule endoscopes, that can be swallowed have previously been developed. However, these devices cannot continuously operate for more than 8 h because of battery limitations; moreover, additional functionalities cannot be introduced. This paper proposes a design method for a high-efficiency energy transmission transformer (ETT) that can transmit energy transcutaneously to small implantable medical devices using electromagnetic induction. First, the authors propose an unconventional design method to develop such a high-efficiency ETT. This method can be readily used to calculate the exact transmission efficiency for changes in the material and design parameters (i.e., the magnetic material, transmission frequency, load resistance, etc.). Next, the ac-to-ac energy transmission efficiency is calculated and compared with experimental measurements. Then, suitable conditions for practical transmission are identified. A maximum efficiency of 33.1% can be obtained at a transmission frequency of 500 kHz and a receiving power of 100 mW for a receiving coil size of ϕ5 mm $\times$ 20 mm. Future design optimization is possible by using this method.**

***Index Terms*—Capsule endoscope, energy transmission, implantable medical device, magnetic material, transmission efficiency.**

I. Introduction

RECENTLY, various types of implantable medical devices, such as a wireless capsule endoscope and a nerve stimulator have been developed [2]–[17]. The M2A [2]–[12] (Given Imaging Ltd.), commercially released in 2001, is a wireless capsule endoscope that is 26 mm long and 11 mm in diameter. The Endo Capsule [17] (Olympus Corp.), which is of the same size, was released in 2005. These capsule endoscopes capture images at 2 frames/s for 8 h using internal batteries. However, other optional functions for capsule endoscopy are necessary, such as sampling or spraying medicine [18]. And if these optional functions are included in a capsule endoscope, its working time reduces. Thus, some methods for supplying energy to a capsule endoscope are needed.

Some researchers have studied the use of wireless energy transmission systems for implantable medical devices. For example, Neagu [19] designed a planar microcoil (air core type) for implantable microsystems, and confirmed that a receiving coil with a diameter of 4.5 mm can receive a few milliwatts. Puers [20]–[22] designed an inductive power-link system for a wireless endoscope, and it became possible to transfer energy up to 50 mW with an efficiency of 36% at a distance of 30 mm (an efficiency of less than 10% at a distance of 70 mm). Morimasa [23] and Hirano [24] developed the air-core-type transformer for implantable medical devices, and their receiving coil 10 mm in diameter could receive 30 mW with an efficiency of 16% at a distance of 100 mm. In this research, however, magnetic material was not adopted and its loss was not considered. To obtain more power and to increase energy transmission efficiency, the introduction of magnetic material into small implantable medical devices is expected. Leuerer [25] developed a planar coil with a magnetic layer for a telemetric system using finite-element method (FEM) analysis, and 4–6 mW of energy could be transferred to the 6-mm diameter receiving coil. However, FEM analysis is time-consuming and expensive, because the designer must make and analyze each model with 2-D or 3-D software. Therefore, for a quick analysis of various types of transformers using various types of magnetic materials at various frequencies, it is not an adequate method. Incidentally, an energy transmission transformer (ETT) for an industrial instrument has already been developed [26]–[29]. For example, Kim *et al.* [26] transmitted about 40 W using a transmitting coil of 3 000 mm^3 and a receiving coil of 2 500 mm^3 at a transmission distance of 3 mm. However, this conventional design method does not consider small magnetic loss and it allows a comparatively large power loss because the industrial transformer is available unless the magnetic material reaches magnetic saturation. Moreover, an industrial transformer is allowed to have a 55–140 °C increase in temperature, because there is no limit except the Curie temperature of the magnetic core or the melting temperature of the electrical insulator [30]. For a capsule endoscope or implantable medical device, the increase in temperature of various parts of the transformer must be in the range of 2 °C–5 °C at most [31].

In this paper, we propose a design method for the bconstruction of an ETT for small implantable medical devices. The design method includes new formulas that accurately express core loss.

II. Energy Transmission System

Fig. 1 shows the energy transmission system for implantable medical devices. The power is transmitted transcutaneously by electromagnetic induction between two coils, one placed inside and the other outside the body. For a wireless capsule endoscope, the receiving coil must have the dimensions ϕ11 mm $\times$ 26 mm [4]. The power consumption of a commercial capsule endoscope is estimated at about 10–30 mW [16] and for optional functions, such as self-propulsion and drug administration

Manuscript received May 18, 2009; revised August 10, 2009. Current version published March 24, 2010. This paper was recommended by Associate Editor R. Sarpeshkar.

The authors are with Graduate school of Engineering, Hiroshima University, Kagamiyama, Hiroshima, 739-8527, Japan (e-mail: kenjishiba@nifty.com; morimasa@bsys.hiroshima-u.ac.jp; harutoyo@bsys.hiroshima-u.ac.jp).

Digital Object Identifier 10.1109/TBCAS.2009.2034364

1932-4545/$26.00 © 2010 IEEE

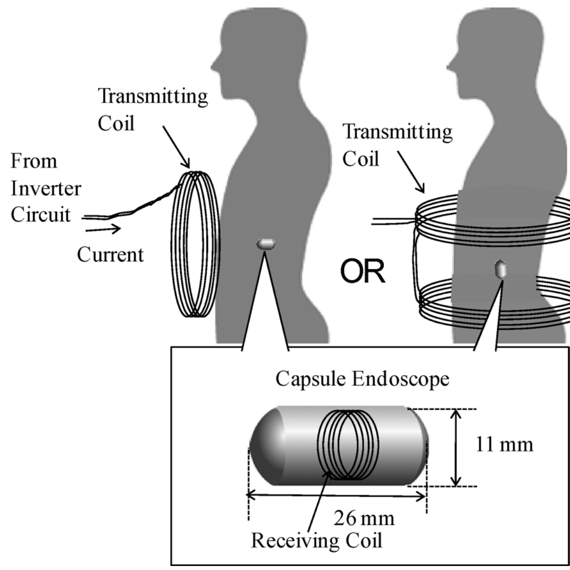

Fig. 1. Parts of an energy transmission transformer.

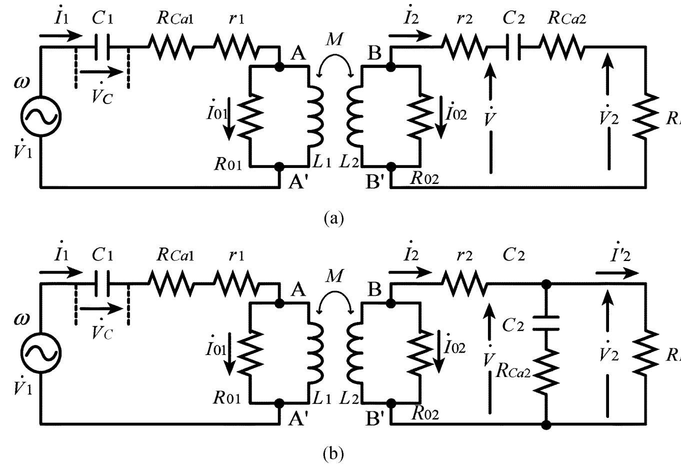

Fig. 2. Equivalent circuits of the energy transmission system. (a) Series resonant circuit. (b) Parallel resonant circuit.

which are included, even greater power (20–900 mW) would be necessary.

III. Design Theory for Transmitting and Receiving Coils

To build a small, high-efficiency receiving coil, magnetic material is desirable on the secondary-coil side. An accurate equivalent circuit that can model the characteristics of a magnetic material is needed in cases where the shape, transmission frequency, magnetic flux density, number of turns, etc., are changed.

A. Equivalent Circuit of Transformer With Core Loss

To transmit a large quantity of power to implantable medical devices, the transformer requires a resonance capacitance with the inductance of the transmitting and receiving coils. Generally, the transmitting side (primary side) is a series resonant circuit, and the receiving side (the secondary side) is a series resonant circuit or a parallel resonant circuit. Fig. 2(a) shows the equivalent series resonant circuits for the ETT, and Fig. 2(b) shows a parallel resonant circuit. In these circuits, ω, V_1 and V_2, r_1 and r_2, L_1 and L_2, C_1 and C_2, R_{Ca1} and R_{Ca2}, M, R_L, and R_{01} and R_{02} represent, respectively, the angular frequency, input and output voltages, transmitting and receiving coil resistances, transmitting and receiving coil inductances, resonant capacitances, equivalent series resistances of the resonant capacitances, mutual inductance, load for the implantable medical device, and core-loss resistances. The circuit equation of Fig. 2(a) is expressed by (1), shown at the bottom of the page. Then, the resonant condition is expressed by

TABLE I
MATERIAL AND DESIGN PARAMETERS OF THE TRANSFORMER

Material parameters		Design parameters
Core loss resistance	$a_s, b_s, c_s, d_s, e_s,$ a_p, b_p, c_p, d_p, e_p	$V_2, R_L, f, d_1, d_2, \theta,$ $a_1, l_1, a_2, l_2, N_1, N_2$
Winding wire	$\alpha_1, \beta_1, \gamma_1,$ $\alpha_2, \beta_2, \gamma_2,$	
Equivalent resistance of capacitor	R_{Ca1}, R_{Ca2}	
Apparent magnetic permeability	$\mu'_{r1}, \mu'_{r2}, \mu'_{rM}$	

$$\omega = \frac{1}{\sqrt{L_1 C_1}} = \frac{1}{\sqrt{L_2 C_2}}. \tag{2}$$

B. Elicitation Process of Core Loss

Core loss P_{i} is equal to the sum of hysteresis loss P_h and eddy-current loss P_e

$$P_i = P_h + P_e. \tag{3}$$

P_h and P_e are expressed as

$$P_h \propto f^u B_m^x, \tag{4}$$

$$P_e \propto f^v B_m^y, \tag{5}$$

$$\begin{bmatrix} r_1 + R_{01} + R_{\mathrm{Ca1}} - j\frac{1}{\omega C_1} & -R_{01} & 0 & 0 \\ -R_{01} & R_{01} + j\omega L_1 & -j\omega M & 0 \\ 0 & -j\omega M & R_{02} + j\omega L_2 & -R_{02} \\ 0 & 0 & -R_{02} & r_2 + R_{02} + R_{Ca2} + R_L - j\frac{1}{\omega C_2} \end{bmatrix} \begin{bmatrix} \dot{I}_1 \\ -\dot{I}_1 - \dot{I}_{01} \\ \dot{I}_2 + \dot{I}_{02} \\ \dot{I}_2 \end{bmatrix} = \begin{bmatrix} \dot{V}_1 \\ 0 \\ 0 \\ 0 \end{bmatrix}. \tag{1}$$

TABLE II
EXPERIMENTAL CONDITIONS AND MAXIMUM EFFICIENCIES OF TYPE I–VII

Type	I	II	III	IV	V	VI	VII
Magnetic material type	A	A	A	B	A	C	C
Load resistance [Ω]	90	90	10	90	90	300	300
Output power [mW]	100	100	900	100	100	30	30
Resonance tpe	Series	Parallel	Series	Series	Series	Series	Parallel
Transmitting coil's diameter [mm]	200	200	200	200	200	300-400	300-400
Receiving coil's diameter [mm]	5	5	5	5	5	10	10
Body condition	In air	In air	In air	In air	In Saline	In air	In air
Maximum efficiency [%] (frequency [kHz])	33.1 (500)	0.3 (70)	9.9 (300)	19.5 (400)	30.4 (500)	19.2 (600)	6.2 (50)

where f is the transmission frequency and B_m is the maximum magnetic flux density. It is known that $u = 0 - 2$, $x = 0 - 2$ (there is sometimes a case where $x \leq 0$ at a ferrite core), $v = 0-2$, and $y = 0-2$ (there is sometimes a case where $y \geq 2$ at a ferrite core) [32]. B_m is proportional to the differential voltage between the terminal voltage of the coil and coil resistance r_2 voltage, V', and inversely proportional to f [33]

$$B_m \propto \frac{V'}{f}. \tag{6}$$

Therefore, P_i is defined as follows:

$$P_i = af^{u-x}V'^x + bf^{v-y}V'^y + c \tag{7}$$

where a, b, and c are constants determined by the magnetic material.

If R_0 is connected in parallel with L_2 as in Fig. 2, by (7), R_0 is expressed by

$$R_0 = \frac{V'^2}{P_i} = \frac{V'^2}{af^{u-x}V'^x + bf^{v-y}V'^y + c}. \tag{8}$$

Using R_{02}, P_{i2} is expressed by

$$P_{i2} = \dot{I}_{02}^2 R_{02}. \tag{9}$$

C. Core-Loss Resistance

In a series resonant circuit, if it is assumed that R_L and V_2 are constant, (8) is transformed as follows because the differential voltage between the terminal voltage of the receiving coil and voltage drop of the coil resistance V' is proportional to f

$$R_0 = \frac{f^2}{a_s f^{d_s} + b_s f^{e_s} + c_s} \tag{10}$$

where $d_s = u = 0 - 2$, $e_s = v = 0 - 2$. In a parallel resonant circuit, (8) is transformed as follows because V' is nearly equal to V_2 when the voltage drop of the secondary coil resistance is smaller than V'

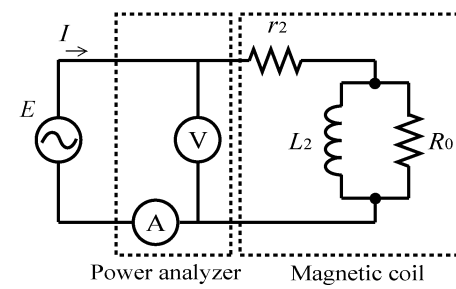

Fig. 3. Measurement circuit for core-loss resistance.

$$R_0 = \frac{1}{a_p f^{d_p} + b_p f^{e_p} + c_p} \tag{11}$$

where $d_p = u - x = -2 - 2$, $e_p = v - y = -2 - 2$ (there is sometimes a case where $e_p \leq -2$ at a ferrite core).

The material parameters (Table I) a_s, b_s, c_s, d_s, and e_s (a_p, b_p, c_p, d_p, and e_p) are proposed by the authors and determined by a one-time measurement. Fig. 3 shows the measurement circuit for the core-loss resistance. The current is applied to the magnetic coil (receiving coil with magnetic material or the transmitting coil with magnetic material); then, the series resistance and the reactance are measured by using equipment, such as a power analyzer or a general-purpose oscilloscope. R_0 is calculated from the real part of the impedance by subtracting the coil resistance. When measuring R_0 using Fig. 3, the supply voltage E in Fig. 3 has to be equal to the actual value of the terminal voltage of the magnetic coil V in Fig. 2. For the series resonant circuit in Fig. 2(a), on the condition that R_{L} and V_2 are constant, the current flowing out of the magnetic coil corresponds to V_2/R_{L}. Therefore, the supply current I in Fig. 3 has to be equal to V_2/R_{L}.

Likewise, for the parallel resonant circuit in Fig. 2(b), on the condition that R_{L} and V_2 are constant, the terminal voltage of the magnetic coil V corresponds to V_2. Therefore, the supply voltage E in Fig. 3 has to be equal to V_2.

a_s, b_s, c_s, d_s, and e_s in (10), or a_p, b_p, c_p, d_p, and e_p in (11) are measured as functions of the transmission frequency.

D. Elicitation Processes for Copper Loss and Capacitor Loss

The transmitting coil's copper loss P_{Co1} (the receiving coil's copper loss P_{Co2}) is defined as the product of $I_1^2(I_2^2)$ and $r_1(r_2)$. r_1 and r_2 are defined as follows because of the skin effect [34]:

$$r_1 = 2\pi a_1 N_1 \left(\frac{f}{\alpha_1\sqrt{f}+\beta_1}+\gamma_1\right) \tag{12}$$

$$r_2 = 2\pi a_2 N_2 \left(\frac{f}{\alpha_2\sqrt{f}+\beta_2}+\gamma_2\right) \tag{13}$$

where N and a are the number of wire turns and the radii, respectively. α_1, β_1, and γ_1 or α_2, β_2, and γ_2 are the material parameters (Table I) determined by the wire type. These material parameters for a 1-m length of litz-wire are measured with equipment, such as an LCR meter, as a function of the transmission frequency.

The losses in the primary-side and secondary-side resonant capacitors P_{Ca1} and P_{Ca2}, respectively, are defined as the products of I_1^2 and R_{Ca1}, and I_2^2 and R_{Ca2}. The equivalent series resistances for the resonant capacitors R_{Ca1} and R_{Ca2} are the material parameters (Table I) determined by the material of the capacitor. R_{Ca1} and R_{Ca2} are measured as functions of the transmission frequency using equipment, such as a general-purpose LCR meter.

E. Self Inductance and Mutual Inductance

The analytical solution of the self-inductance is used in (1) and (2). The self-inductance of the transmitting and receiving coils can be calculated by a simplified numerical analysis [35]. When the calculation is very complex, depending on the layout of the magnetic material, the self-inductance is calculated based on a measured result. The self-inductance of a coil with magnetic material L' is defined as multiplication between the apparent relative magnetic permeability μ_r' and the self-inductance of the coil without the magnetic material L. The mutual inductance between the transmitting and receiving coils M can be calculated by using Neumann's law when considering the shape or relative positions of the coils [35]. In order to calculate the mutual inductance with magnetic material M', the apparent relative magnetic permeability μ_{rM}' has to be derived by using the onetime measured M' divided by the calculated M (from Neumann's law) or the onetime measured M.

F. Energy Transmission Efficiency

The energy transmission efficiency η is expressed by

$$\eta = \frac{P_2}{P_{i2}+P_{\mathrm{Co1}}+P_{\mathrm{Co2}}+P_{\mathrm{Ca1}}+P_{\mathrm{Ca2}}+P_2} \tag{14}$$

where P_2 is the output power, which is defined as V_2^2 divided by R_L, P_{i2} is the core loss of the receiving coil, P_{Co1} is the transmitting coil's copper loss, P_{Co2} is the receiving coil's copper loss, P_{Ca1} is the loss in the primary-side resonance capacitance, and P_{Ca2} is the loss in the secondary-side resonance capacitance. In this paper, the ETT is optimally designed by maximizing the efficiency η.

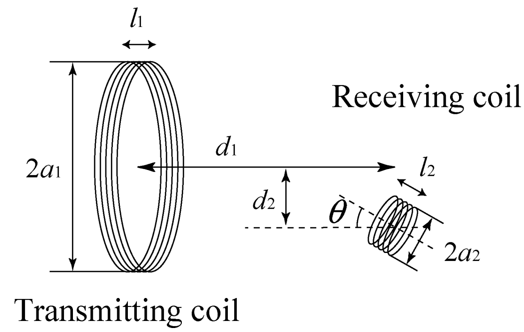

Fig. 4. Arrangement of the two coils.

In the design process, first, the material parameters shown in Table I are measured or specified, and then, the transmission efficiency is optimized in terms of the design parameters defined by the user for the given constraints by using (14). Table I shows a list of candidate design parameters from which the user can choose the necessary ones. The ETT can be designed on the basis of the proposed design theory.

IV. Design Example of the Transmitting and Receiving Coils

As an example, transmitting and receiving coils that are wound with the same circumference were designed for the case where f, l_2, and d_1 change. In this calculation, the output voltage was set at 3 V, and $d_2 = 0$ cm and $\theta = 0$ rad in Fig. 4. The transmitting coils of types I–V had a diameter $2a_1$ of 20 cm and a length l_1 of 3 cm [Figs. 1 and 5(a)]. The receiving coils of types I–V had a diameter $2a_2$ of 5 mm and a length l_2 of 2 cm. In addition, the length of the coils l_1 and l_2 change due to N_1 and N_2. The number of wire turns per unit length N_1' and N_2' were set at 75 turns/cm and 7.5 turns/cm, respectively.

The transmitting coils of types VI–VII comprised series-connected double solenoidal coils [Fig. 1 and Fig. 5(b)]. Each solenoidal coil had a diameter $2a_1$ of 30–40 cm (ellipse) and a length l_1 of 6 cm. The distance between the two coils was 20 cm. The receiving coils of types VI–VII had a diameter $2a_2$ of 10 mm and a length l_2 of 2 cm. N_1' and N_2' for types VI–VII were set at 4 turns/cm and 47.5 turns/cm, respectively.

A. Measurement of the Material Parameters

First, the material parameters in Table I were measured. The prototype receiving coils of types I–V (Fig. 5) had 150 turns of litz-wire (UEW wire, bundles of 15 wires of ϕ0.03 mm) wound around Material A (EPCOS AG, K1) or Material B (Hitachi Metals Ltd., FINEMET). Material A is a cylindrical ferrite core. Material B is a fivefold-thinner amorphous magnetic material sheet (0.3-mm (thickness) $\times$ 5) wound around a wooden stick with a diameter of 2 mm. The prototype receiving coils of types VI–VII (Fig. 5) had 95 turns of single-wire (UEW wire, ϕ0.2 mm) wound around Material C (a thin amorphous magnetic sheet, 0.03 mm in thickness) wound around a wooden stick

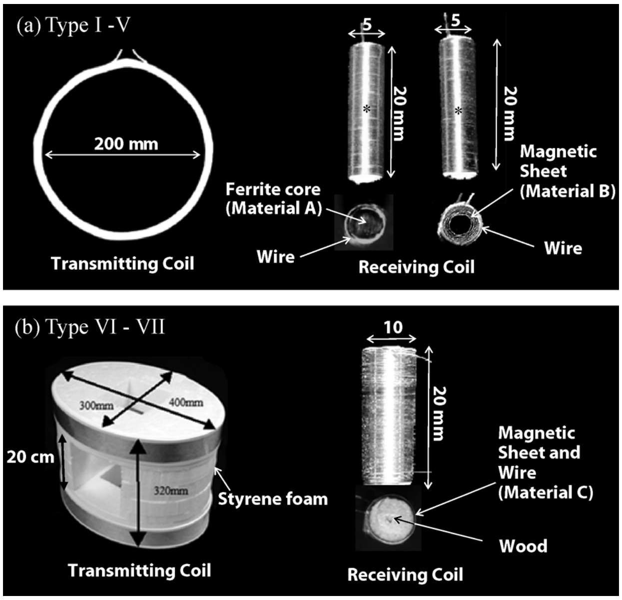

Fig. 5. Transmitting coil and receiving coil of (a) types I–V and (b) types VI–VII.

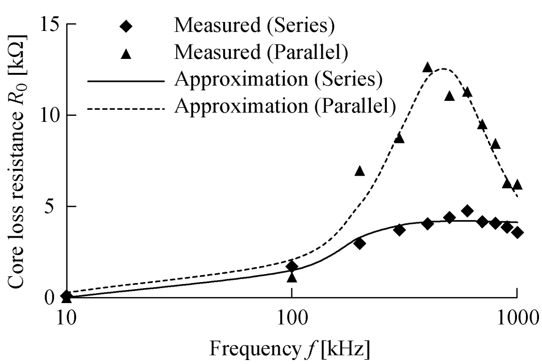

Fig. 6. Measured results versus approximation of the core-loss resistance.

with a diameter of 2.5 mm. A wooden stick is used only to fasten the thin amorphous magnetic sheet.

The core-loss resistances for the receiving coils were measured by using a power analyzer (Yokogawa Electric Corp., PZ4000) at transmission frequencies of 10 kHz to 1 MHz. Fig. 6 shows the measured R_0 values for Material A and an approximation fitted to (10) and (11) by the least-squares method (using Mathematica 6.0). From the measured results, the material parameters for the core-loss resistance of Material A were $a_s = -2.3$, $b_s = 2.6 \times 10^{-5}$, $c_s = 6.3 \times 10^5$, $d_s = 1.0$, $e_s = 2.0$, $a_p = 0.1$, $b_p = 3.9 \times 10^{-9}$, $c_p = -7.0 \times 10^{-5}$, $d_p = -0.6$, and $e_p = 0.7$. The material parameters for the core-loss resistances of Materials B and C are as follows: $a_s = -5.3$, $b_s = 5.7 \times 10^{-5}$, $c_s = 8.8 \times 10^5$, $d_s = 1.0$, $e_s = 2.0$, $a_p = -2.4 \times 10^{-12}$, $b_p = 1.7$, $c_p = 5.2 \times 10^{-5}$, $d_p = 1.0$, and $e_p = -1.0$ (Material B); and $a_s = 1.8 \times 10^{-4}$, $b_s = 6.9$, $c_s = 1.7 \times 10^6$, $d_s = 2.0$, $e_s = 1.0$, $a_p = 4.4 \times 10^{-8}$, $b_p = 1.8$, $c_p = -8.6 \times 10^{-5}$, $d_p = 0.6$, $e_p = -0.7$ (Material C).

Then, the resistance of the litz-wire (UEW wire; types I–V, bundles of 360 wires of ϕ0.05 mm for the transmitting coil and bundles of 15 wires of ϕ0.03 mm for the receiving coil; types VI–VII, bundles of 798 wires of ϕ0.05 mm for the transmitting coil and single wires of ϕ0.2 mm for the receiving coil) was measured by using an LCR meter (HIOKI E. E. Corp., 3532-50). The material parameters of the winding wire were $\alpha_1 = -1.2 \times 10^5$, $\beta_1 = 1.4 \times 10^8$, $\gamma_1 = 1.9 \times 10^{-3}$, $\alpha_2 = 7.4 \times 10^4$, $\beta_2 = -1.8 \times 10^6$, and $\gamma_2 = 1.7$ (types I–V) and $\alpha_1 = 5.7 \times 10^4$, $\beta_1 = 7.7 \times 10^{-2}$, $\gamma_1 = 1.2 \times 10^{-2}$, $\alpha_2 = -2.5 \times 10^3$, $\beta_2 = 4.4 \times 10^{-6}$, and $\gamma_2 = 5.6 \times 10^{-1}$ (types VI–VII).

The material parameters of the equivalent series resistances of resonant capacitances R_{Ca1} and R_{Ca2} of types I–V were set at 0.25 Ω from the measurement results for the polypropylene capacitor used (Evox Rifa, PHE450) at a transmission frequency of 100 kHz. R_{Ca1} and R_{Ca2} for types VI–VII were, respectively, set at 0.30 Ω and 0.25 Ω from the measurement results for the polypropylene capacitor used (C_1: Evox Rifa, PHE450; C_2: NISSEI Electric, MPE1600J) at a transmission frequency of 100 kHz.

The material parameter of the apparent relative magnetic permeability μ'_{r1} of types I–VII was 1.0 because the transmitting coil had an air core. μ'_{r2} for Material A was found to be 18.0 from the measurement results ($L' = 450.5\ \mu$H) obtained by using an LCR meter (HIOKI E. E. Corp., 3532-50), along with the calculated result ($L = 25.0\ \mu$H). L was calculated by using the Nagaoka coefficient K [35] due to the solenoidal coil. μ'_{r2} for Materials B and C was 20.07 and 6.19, respectively. These values were calculated by one-time measurements.

M' for Material A in types I–V was calculated by using the prototype transmitting and receiving coils, as described in Section III-E. d_1, d_2, and θ were set at 10 cm, 0 cm, and 0 rad, respectively. From the results—$M' = 1.8\ \mu$H and $M = 98.0$ nH—μ'_{rM} was calculated to be 18.1. μ'_{rM} for Materials B and C in types I–VII was calculated by using a one-time measurement of M and M'. The measured value of μ'_{rM} for Materials B and C is 20.2 and 10.7, respectively.

B. Calculations of the Transmission Efficiency, Core Loss, and Copper Loss of Receiving Coil

The transmission efficiency of the type I (Material A) system was calculated by using the material parameters in Section IV-A for a series resonant circuit, $V_2 = 3$ V, $R_L = 90\ \Omega$, $P_2 = 100$ mW, and $d_1 = 10$ cm. The capsule endoscope must be of a swallowable size. In addition, the terminal voltage of the resonant capacitor must have a realistic value that is less than the maximum voltage [37], [38]. Therefore, the limit is set as follows:

$$l_2 \leq 20 \text{ mm} \tag{15}$$

$$V_C \leq 700 \text{ V}. \tag{16}$$

The above equation sets the design conditions for the example capsule endoscope.

Fig. 7 shows an example of the calculated results when f and l_2 change. The maximum efficiency η was 24.5% at $l_2 = 20.0$ mm and $f = 477.1$ kHz. The equation for the efficiency is shown in Appendix B. Fig. 8 shows a partial differential of the efficiency $\partial\eta/\partial f$ at $l_2 = 20$ mm and 10 mm (example of a downsized type I system). For $l_2 = 10$ mm, $\partial\eta/\partial f$ is 0 at $f = 627.5$ kHz. For $l_2 = 20$ mm, $\partial\eta/\partial f$ is 0 at $f = 477.1$ kHz. The transmission frequency at which $\partial\eta/\partial f$ becomes 0 is the same

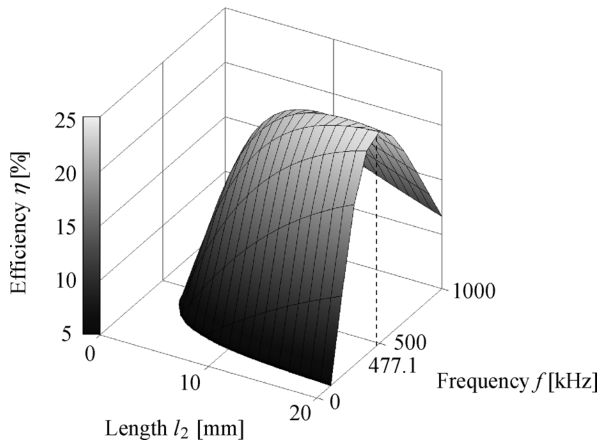

Fig. 7. Calculated efficiency for type I.

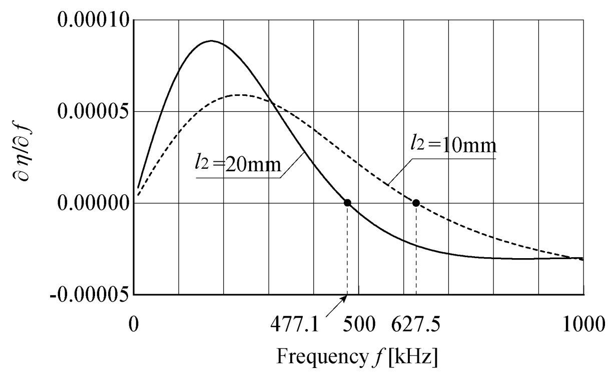

Fig. 8. Calculated $\partial\eta/\partial f$ for type I.

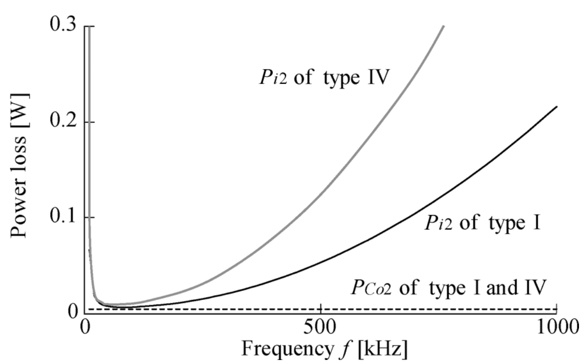

Fig. 9. Calculated core loss and copper loss for types I and IV.

as the optimal transmission frequency in Fig. 7. Thus, it is easily possible to design an optimal transformer.

Then, the receiving coil's core loss P_{i2} for types I and IV and the receiving coil's copper loss $P_{\mathrm{Co}2}$ for type I were calculated at transmission frequencies of 10 kHz to 1 MHz and a receiving coil length of 20 mm. Fig. 9 shows the calculated results. The core loss P_{i2} of types I and IV increased with the transmission frequency above 100 kHz, and reached an approximate power loss of 0.2 W at 1 MHz and 600 kHz, respectively. However, the receiving coil's copper loss $P_{\mathrm{Co}2}$ for types I and IV was a constant power loss of about 4 mW. The designer can easily find that the core loss P_{i2} is 2–100 times as large as $P_{\mathrm{Co}2}$ from Fig. 9.

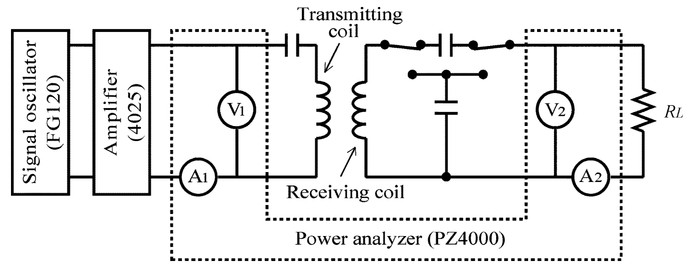

Fig. 10. Measurement circuit for efficiency.

C. Experimental Measurement of Transmission Efficiency

To validate this design method, an experimental measurement of the transmission efficiency was conducted. Fig. 10 shows the measurement circuit used. The transmitting and receiving coils are shown in Fig. 5. The ac voltage output from a signal oscillator (Yokogawa Electric Corp., FG120) was amplified by a high-speed amplifier (NF Electronic Instruments, 4025) and transferred to the receiving coil by the transmitting coil through air or saline. A metal-coated noninductive resistor (error of 1%) was used as the load resistance R_L, and V_2 was set at 3 V. The energy transmission efficiency η was measured at transmission frequencies of 100–600 kHz (due to limitations in the measuring equipment) in 100-kHz increments by using a power analyzer (Yokogawa Electric Corp., PZ4000).

Fig. 11(a) shows the measured and calculated results for $d_1 =$ 10 cm and the type I (Material A, $R_L = 90\ \Omega$, $P_2 = 100$ mW, with a series resonant circuit), type II (Material A, $R_L =$ 90 Ω, with a parallel resonant circuit), type III (Material A, $R_L = 10\ \Omega$, $P_2 = 0.9$ W, with a series resonant circuit), type IV (Material B, $R_L = 90\ \Omega$, with a series resonant circuit), and type V (receiving coil of type I placed in saline water) systems. Fig. 11(b) shows the measured and calculated results of the efficiency of the type VI (Material C, $R_L = 300\ \Omega$, $P_2 = 30\ \mathrm{mW}$, with a series resonant circuit) and type VII (Material C, $R_L = 300\ \Omega$, with a parallel resonant circuit) systems.

The maximum efficiency of types I, II, III, and IV are, respectively, 33.1% at 500 kHz, 0.3% at 70 kHz, 9.9% at 300 kHz, and 19.5% at 400 kHz. The maximum efficiency of types VI and VII are, respectively, 19.2% at 600 kHz and 6.2% at 50 kHz. Types I and VI achieve the highest efficiency. From the results for types I and V, we see that there was no attenuation in saline at frequencies less than 600 kHz [Fig. 11(a)].

Fig. 12 shows the results for the type I (Material A, $R_L =$ 90 Ω, with a series resonant circuit) system when d_1 and frequency change. Fig. 13 shows the terminal voltage of the resonance capacitor C_1 for types I–IV. All of these calculated results are roughly in accordance with the measured results.

D. Experimental Measurement of the Temperature

The temperatures of the receiving coils in types I, IV, and VI in Section IV-C were measured at transmission frequencies of 100–600 kHz. A data logger (M-System Co., Ltd., R2M-2H3) recorded the steady-state temperature after a lapse of 5 min. The experimental measurement was conducted in a constant-temperature bath (TOKYO RIKAKIKAI Co., Ltd., NTT-2000) to keep the temperature at 37 °C. A thermocouple (Type J) was

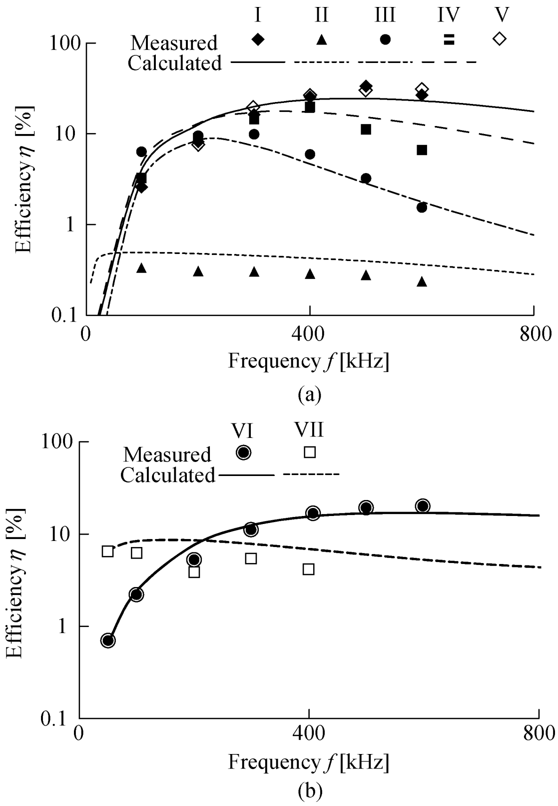

Fig. 11. Calculated results and measured results of the efficiency for (a) type I (Material A, $R_L = 90\ \Omega$, $P_2 = 100$ mW, with a series resonant circuit), type II (Material A, $R_L = 90\ \Omega$, with a parallel resonant circuit), type III (Material A, $R_L = 10\ \Omega$, $P_2 = 0.9$ W, with a series resonant circuit), type IV (Material B, $R_L = 90\ \Omega$, with a series resonant circuit), and type V (receiving coil of type I placed in saline water), and (b) type VI (Material C, $R_L = 300\ \Omega$, $P_2 = 30$ mW, with a series resonant circuit) and type VII (Material C, $R_L = 300\ \Omega$, with a parallel resonant circuit).

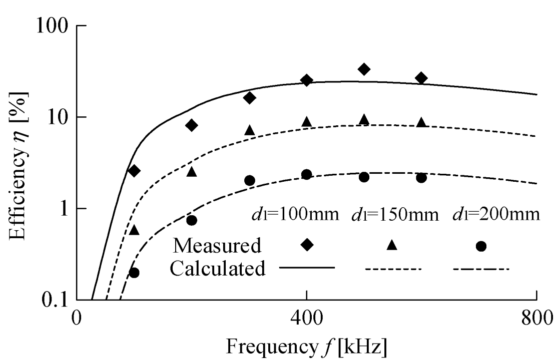

Fig. 12. Calculated and measured results of the efficiency for change in transmission distance.

used as a temperature sensor. The asterisk in Fig. 5 shows the measurement point. Fig. 14 shows the measured temperature results as a function of the transmission frequency. The steady-state temperature for type IV was 45.3 °C, which is a high value. However, the temperature at a transmission frequency of 600 kHz for types I and VI was, respectively, 39.6 °C and 37.5 °C, being about 6 °C–8 °C smaller than that for type IV.

V. DISCUSSION

The results in Fig. 6 show that the proposed formulas for the core-loss resistance [(10) and (11)] are valid because the material parameters $a_s - e_s$ and $a_p - e_p$ are appropriate, as determined by conventional research [32].

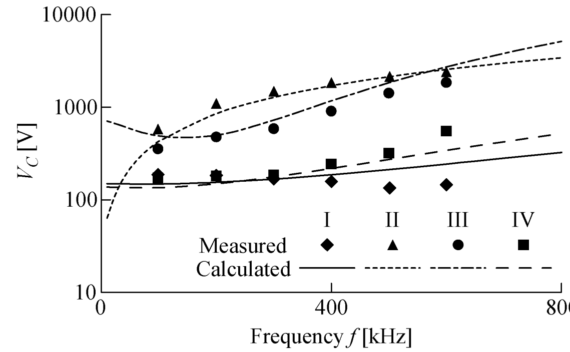

Fig. 13. Calculated and measured VC for types I–V.

The results of Fig. 7 show that the optimal value of the transmission frequency depends on l_2. To design a receiving coil that can be swallowed, it is necessary to choose the transmission frequency in accordance with the coil length. This design method is very useful since it allows the creation of an optimal design without the need for fabricating a real device. When only a variable parameter exists, the optimization is easily performed, as in Fig. 8.

In addition, the results shown in Fig. 11 confirm that f and l_2 depend on R_L and the resonant circuit. In this case, an optimal design is also possible with numerical calculation.

For types I and II, the maximum efficiency is only 0.3% while the maximum efficiency of type I was 33.1%. For the discrepancy in efficiency between types I and II, the capacitor loss P_{ca1} is very large in type II (P_{ca1} of type II at 600 kHz is 17.8 W, while P_{ca1} of type I is 0.16 W) because the terminal voltage of the resonance capacitor shows a very high value (see Fig. 13).

Figs. 11 and 12 show the accordance between the calculated and measured results. Therefore, the equivalent circuit and measurement method for the core loss are considered to be accurate. In this study, we confirmed that the type I system could provide a higher efficiency than type IV. ($\eta = 24.4\%$ for type I and $\eta = 15.2\%$ for type IV at a transmission frequency of 500 kHz). However, the results of conventional analysis [23] show that type IV is more efficient than type I ($\eta = 46.5\%$ for type I and $\eta = 51.9\%$ for type IV at 500 kHz). It seems that our new analysis method is useful not only for the design of implantable medical devices, but also for the design of various industrial devices.

Fig. 9 shows that the core loss P_{i2} of types I and IV increased with the transmission frequency. In addition, Fig. 14 shows that the temperature of types I and IV increased with the transmission frequency, though the transmission efficiency reached a maximum value at a transmission frequency of about 500 kHz and 300–400 kHz, respectively (Fig. 11). The efficiency is not proportional to the temperature. Form this result, to design implantable devices, we find that the ability to rapidly and accurately calculate not only efficiency but also power losses in various parts, such as the core loss, copper loss in the receiving coil, and loss in the resonance capacitor, is important. For these reasons, our method is very valuable for the development of ETTs for implantable devices.

As for the temperature, it is well known that a temperature of 42.5 °C causes heat injury to biological tissue [31]. Therefore,

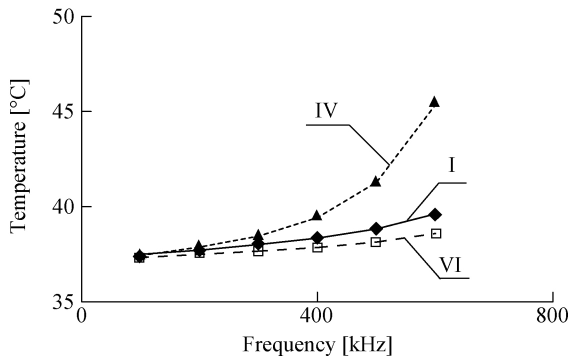

Fig. 14. Measured temperatures of types I, IV, and VI.

the receiving coil of type IV cannot be easily used because of its high temperature of more than 45.3 °C at 600 kHz. On the other hand, it is possible to use the receiving coil of types I and VI for a capsule endoscope or implantable medical device due to the low temperature of 37.5 °C–39.6 °C at 100–600 kHz.

Compared with conventional studies, type I of our transformer can achieve the highest efficiency for the condition of a distance of 100 mm and a receiving coil size of $\phi 5$ mm $\times$ 20mm.

When a transformer is actually designed, it is expected that the design parameters will include many more constraints. However, it is possible to design an optimal transformer by using this method.

VI. Conclusion

In this paper, we proposed an unconventional design method for a high-efficiency ETT for a small implantable medical device. This method can be used to calculate the transmission efficiency in a rapid and accurate manner when the magnetic material of the ETT, transmission frequency, load resistance, etc., are changed. Our experiments confirmed the validity of the calculated results and, thus, the validity of our design method.

In the future, we will design ETTs for implantable medical devices with even higher efficiency and smaller size by exploring the various kinds of magnetic materials that are usable.

Appendix A
Mutual Inductance of the Solenoidal Coil

The solenoidal coil's M' is expressed by

$$M'(\theta, a_1, a_2, d_1, d_2, N_1, N_2) = \mu'_{rM} M, \tag{A1}$$

$$\begin{aligned} M &= \mu_0 \sqrt{a_1} a_2^2 N_1 N_2 \\ &\times \left[-\frac{\partial \frac{1}{k\sqrt{d_2}} \left\{ \left(1 - \frac{k^2}{2}\right) K(k) - E(k) \right\}}{\partial d_1} \sin\theta \right. \\ &\left. + \frac{1}{d_2} \frac{\partial \frac{\sqrt{d_2}}{k} \left\{ \left(1 - \frac{k^2}{2}\right) K(k) - E(k) \right\}}{\partial d_2} \cos\theta \right] \end{aligned} \tag{A2}$$

where N'_1 and N'_2 are, respectively, the number of turns per meter length of the transmitting and receiving coils; a_1 and a_2 are, respectively, the diameters of the transmitting and receiving coils; μ_0 is the permeability of vacuum; d_1 is the distance between the transmitting and receiving coils; d_2 is the distance between the transmitting and receiving coil axes; θ is the inclination angle from the coil axis; $K(k)$ is the complete elliptic integral of the first kind; $E(k)$ is the complete elliptic integral of the second kind; and k is expressed by

$$k = \sqrt{\frac{4a_1 d_2}{(a_1 + d_2)^2 + d_1^2}}. \tag{A3}$$

In addition, M' is simply expressed as follows in a case where $d_2 = 0$ and $\theta = 0$ [32]:

$$M'(a_1, a_2, d_1, N_1, N_2) = \mu'_{rM} M, \tag{A4}$$

$$M = \frac{\mu_0 \pi a_1^2 a_2^2 N_1 N_2}{2\left(a_1^2 + d_1^2\right)^{3/2}}. \tag{A5}$$

In this case, M' and M are expressed as functions of a_1, a_2, d_1, N_1, and N_2.

Appendix B
Energy Transmission Efficiency

The equation for the energy transmission efficiency is expressed by

$$\begin{aligned} \eta = I_2^2 R_L \Bigg/ \Bigg\{ & \frac{\dot{I}_{02} f^2}{a_s f^{d_s} + b_s f^{e_s} + c_s} \\ & + 2\pi a_1 I_1^2 N_1 \left(\frac{f}{\alpha_1 \sqrt{f} + \beta_1} + \gamma_1 \right) \\ & + 2\pi a_2 I_2^2 N_2 \left(\frac{f}{\alpha_2 \sqrt{f} + \beta_2} + \gamma_2 \right) \\ & + I_1^2 R_{Ca1} + I_2^2 R_{Ca2} + I_2^2 R_L \Bigg\} \end{aligned} \tag{A6}$$

where I_1 is the input current, I_2 is the output current, and I_{02} is the current through the core-loss resistance R_{02} in Fig. 2(a). These currents are expressed as follows:

$$\begin{aligned} I_1 = \Bigg| -j\dot{V}_2 \Bigg[& \frac{f^2}{a_s f^{d_s} + b_s f^{e_s} + c_s} \\ & \times \left\{ 2\pi a_2 N_2 \left(\frac{f}{\alpha_2 \sqrt{f} + \beta_2} + \gamma_2 \right) \right. \\ & \left. + R_{Ca2} + R_L \right\} + j2\pi \mu'_{r2} f L_2 \\ & \times \left\{ 2\pi a_2 N_2 \left(\frac{f}{\alpha_2 \sqrt{f} + \beta_2} + \gamma_2 \right) + R_{Ca2} \right. \\ & \left. + R_L - j2\pi \mu'_{r2} f L_2 \right\} \Bigg] \\ & \Bigg/ \frac{2\pi \mu'_{rM} f^3 M R_L}{a_s f^{d_s} + b_s f^{e_s} + c_s} \Bigg|, \end{aligned} \tag{A7}$$

$$I_2 = \left| \frac{\dot{V}_2}{R_L} \right|, \tag{A8}$$

$$\begin{aligned} I_{02} = \Bigg| \Bigg[\dot{V}_2 \Bigg\{ & 2\pi a_2 N_2 \left(\frac{f}{\alpha_2 \sqrt{f} + \beta_2} + \gamma_2 \right) \\ & + \frac{f^2}{a_s f^{d_s} + b_s f^{e_s} + c_s} + R_{Ca2} \\ & + R_L - j2\pi \mu'_{r2} f L_2 \Bigg\} \\ & \Bigg/ \frac{f^2 R_L}{a_s f^{d_s} + b_s f^{e_s} + c_s} \Bigg] - \frac{\dot{V}_2}{R_L} \Bigg|. \end{aligned} \tag{A9}$$

REFERENCES

[1] H. Yamamoto, H. Kita, K. Sunada, T. Yano, Y. Hayashi, H. Sato, H. Ajibe, M. Iwamoto, K. Ido, and K. Sugano, "Current status of enteroscopy," *Gastro. Endoscopy*, vol. 47, no. 10, pp. 2353–2360, 2005.

[2] G. Iddan, G. Meron, A. Glukhovsky, and P. Swain, "Wireless capsule endoscopy," *Nature*, vol. 405, p. 417, 2000.

[3] G. Meron, "The development of the swallowable video capsule (M2A)," *Gastro. Endoscopy*, vol. 52, no. 6, pp. 817–819, 2000.

[4] W. A. Qureshi, "Current and future applications of the capsule camera," *Nature Rev. Drug Discov.*, vol. 3, pp. 447–450, 2004.

[5] Z. Fireman, E. Mahajna, E. Broide, M. Shapiro, L. Fich, A. Sternberg, Y. Kopelman, and E. Scapa, "Diagnosing small bowel Crohn's disease with wireless capsule endoscopy," *Gut*, vol. 52, pp. 390–392, 2003.

[6] E. Scapa, H. Jacob, S. Lewkowicz, M. Migdal, D. Gat, A. Gluck-hovski, N. Gutmann, and Z. Fireman, "Initial experience of wireless-capsule endoscopy for evaluating occult gastrointestinal bleeding and suspected small bowel pathology," *Amer. J. Gastro.*, vol. 97, no. 11, pp. 2776–2779, 2002.

[7] S. Liangpunsakul, V. Chadalawada, D. K. Rex, D. Maglinte, and J. Lappas, "Wireless capsule endoscopy detects small bowel ulcers in patients with normal results from state of the art enteroclysis," *Amer. J. Gastro.*, vol. 98, no. 6, pp. 1295–1298, 2003.

[8] M. Mylonaki, A. Fritscher-Ravens, and P. Swain, "Wireless capsule endoscopy: A comparison with push enteroscopy in patients with gastroscopy and colonoscopy negative gastrointestinal bleeding," *Gut*, vol. 52, pp. 1122–1126, 2003.

[9] R. Eliakim, "Wireless capsule video endoscopy: Three years of experience," *World J.Gastro.*, vol. 10, no. 9, pp. 1238–1239, 2004.

[10] N. Dai, C. Gubler, P. Hengstler, C. Meyenberger, and P. Bauerfeind, "Improved capsule endoscopy after bowel preparation," *Gastrointest. Endoscopy*, vol. 61, no. 1, pp. 28–31, 2005.

[11] W. Selby, "Complete small-bowel transit in patients undergoing capsule endoscopy: Determining factors and improvement with metoclopramide," *Gastrointest. Endoscopy*, vol. 61, no. 1, pp. 80–85, 2005.

[12] A. K. H. Chong, A. C. F. Taylor, A. M. Miller, and P. V. Desmond, "Initial experience with capsule endoscopy at a major referral hospital," *Med. J. Australia*, vol. 178, pp. 537–540, 2003.

[13] J. H. Lee, H. J. Park, Y. K. Moon, B. S. Song, C. H. Won, H. C. Choi, J. T. Lee, and J. H. Cho, "Design and implementation of the CPLD controller for Bi-directional wireless capsule endoscopy," in *Proc. Int. Tech. Conf. Circuits/Systems, Computers and Communications*, Miyagi, Japan, Jul. 2004, pp. 7F3P-67-1–7F3P-67-4.

[14] D. Turgis and R. Puers, "Image compression in video radio transmission for capsule endoscopy," presented at the Eurosensors XVIII, Rome, Italy, Sep. 2004.

[15] V. S. Kodogiannis, M. Boulougoura, and E. Wadge, "The usage of soft-computing methodologies in interpreting capsule endoscopy," in *Comput. Biol. Med.*. New York: Elsevier, 2004.

[16] X. Xie, G. Li, B. Chi, X. Yu, C. Zhang, and Z. Wang, "Micro-system design for wireless endoscopy system," in *Proc. IEEE 27th Annu. Conf. Engineering in Medicine and Biology* , Shanghi, China, Sep. 2005, pp. 7135–7138.

[17] "Olympus launches high-resolution capsule endoscope in Europe—The capsule endoscope system for small bowel which allows real time observation." Olympus Corp. Tokyo, Japan. [Online]. Available: http://www.olympus-global.com/en/news/2005b/nr051013capsle.cfm?chm=4

[18] Strategic Technology Roadmap 2007 Ministry of Economy, Trade and Industry. [Online]. Available: http://www.meti.go.jp/policy/kenkyu_kaihatu/trm/TRM2007/trm2007.htm, 2007

[19] C. R. Neagu, H. V. Jansen, A. Smith, J. G. E. Gardeniers, and M. C. Elwenspoek, "Characterization of a planar microcoil for implantable microsystems," *Sensors Actuators A*, vol. 62, pp. 599–611, 1997.

[20] M. Catrysse, B. Hermans, and R. Puers, "An inductive power system with integrated bi-directional data-transmission," *Sensors Actuators A*, vol. 115, no. 2–3, pp. 221–229, 2004.

[21] B. Lenaerts and R. Puers, "Inductive powering of a freely moving system," *Sensors Actuators A*, vol. 123–124, pp. 522–530, 2005.

[22] B. Lenaerts and R. Puers, "An inductive power link for a wireless endoscope," *Biosensors Bioelectron.*, vol. 22, no. 7, pp. 1390–1395, 2007.

[23] A. Morimasa, T. Nagato, K. Shiba, and T. Tsuji, "Energy transmission system for endoscopy capsule—An attempt to improve the transmission ability," in *Proc. 21st Ann. Conf. Soc. Life Support Technology*, Mie, Japan, Dec. 2005, p. 50.

[24] H. Hirano, A. Morimasa, K. Shiba, and T. Toshio, "Design of capsule endoscope transcutaneous energy transmission system," IEICE Tech. Rep. MBE2007-131, 2008, pp. 105–108.

[25] T. Leuerer and W. Mokwa, "Planar coils with magnetic layers for optimized energy transfer in telemetric systems," *Sensors Actuators A*, vol. 116, pp. 410–416, 2004.

[26] C. G. Kim, D. H. Seo, J. S. You, J. H. Park, and B. H. Cho, "Design of a contactless battery charger for cellular phone," *IEEE Trans. Ind. Electron.*, vol. 48, no. 6, pp. 1238–1247, Dec. 2001.

[27] A. Hasegawa, *Know-How on Engineering Switching Regulator*. Tokyo, Japan: CQ, 1993.

[28] *Fundamentals of Electric Measurement*. Tokyo: Ohmsha Ltd., 2000, pp. 121–140, Inst. Elect. Eng. Jpn.

[29] *IEEE Standard for Test Procedures for Magnetic Cores,*, Std. 393-1977, IEEE Power Electron. Soc., 1992.

[30] Inst. Elect. Eng. Japan-Japanese Electrotech Committee, *Transfomer*. Tokyo, Japan: Denkishoin Co. Ltd., 1995, JEC-2200 1995.

[31] Japan Soc.Med. Electron. >Biol. Eng., *Basic Knowledge and Safety Management of Medical and Biological Engineering*, 4th ed. Tokyo, Japan: Nankodo Co. Ltd., 2002, pp. 42–60.

[32] Y. Sasaki and T. Sato, "Large signal eddy current losses beyond 100 kHz," *IEEE Trans. Magn.*, vol. MAG-31, no. 5, pp. 1487–1489, Sep. 1984.

[33] *Electrical Machines Engineering I*, Revised ed. Tokyo: Ohmsha, Ltd., 1999, pp. 79–160, Inst. Elect. Eng. Jpn.

[34] S. Omori, I. Yokoshima, and H. Nakane, *High Frequency and Microwave Measurements*. Tokyo, Japan: Corona, 1992, pp. 7–8.

[35] R. Aoki, Inst. Elect. Eng. Jpn., *Electrical Engineering Handbook*, 6th ed. Tokyo, Japan: Ohmsha, 2001, pp. 64–68.

[36] K. Goto and S. Yamazaki, *Exercises in Electromagnetism Interpreted in Detail*. Tokyo, Japan: Kyoritsu Shuppan , 1970, pp. 271–291.

[37] Film and ceramic capacitors. Evox Rifa. . Espoo, Finland. [Online]. Available: http://www.evox-rifa.com/europe/film_capacitor_catalog.htm

[38] Passive&Electromechanical-Film Capacitors Matsushita Electric Industrial Co. Ltd. Tokyo, Japan. [Online]. Available: http://industrial.panasonic.com/www-ctlg/ctlg/qABD0000_WW.html

Kenji Shiba (M'00) received the B.E., M.E., and D.E. degrees in electrical engineering from the Tokyo University of Science, Chiba, Japan, in 1995, 1997, and 2000, respectively.

From 2000 to 2001, he was a Research Fellow at the Japan Society for the Promotion of Science. In 2001, he joined the Department of Human and Engineered Environmental Studies at the University of Tokyo as a Research Associate. In 2002, he returned to Tokyo University of Science as a Research Associate. In 2004, he joined the Department of Artificial Complex Systems at Hiroshima University, where he is an Associate Professor. His current research interests include the development of implantable medical devices, bioelectromagnetics, and electromagnetic compatibility.

Dr. Shiba won the Best Paper Award from the Japanese Society for Artificial Organs in 2001. He is a member of the Japanese Society for Artificial Organs, the Japan Society of Medical Electronics and Biological Engineering, the IEEE Engineering in Medicine and Biology Society, and the IEEE Electromagnetic Compatibility Society.

Akira Morimasa received the B.E. degree in electrical, computer, and systems engineering from Hiroshima University, Hiroshima, Japan, in 2006 and the M.E. degree in artificial complex systems engineering from Hiroshima University in 2008.

His research interest includes the transcutaneous energy transmission system for a wireless capsule endoscope.

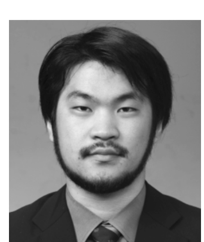

Harutoyo Hirano received the B.E. degree in electrical, computer, and systems engineering from Hiroshima University, Hiroshima, Japan, in 2008, where he is currently pursuing the M.Sc. degree in artificial complex systems engineering.

Currently, he is with Hiroshima University. His research interest includes a transcutaneous energy transmission system for implantable medical devices.